actuators

MDPI

Article

A Comprehensive Experimental–Analytical Framework for Motorcycle Testing with Fourier-Based Curve Fitting and Adaptive Control

Firat Can Yilmaz [1], Muzaffer Metin [2,*] and Talha Oguz [2,3]

[1] Department of Mechanical Engineering, Gebze Technical University, Kocaeli 41400, Türkiye; fcyilmaz@gtu.edu.tr
[2] Department of Mechanical Engineering, Yildiz Technical University, Istanbul 34349, Türkiye; talha.oguz@mert.com
[3] Research and Development Centre, Mert Teknik Fabrika Malzemeleri Ticaret ve Sanayi A.Ş., Istanbul 34775, Türkiye
* Correspondence: mmetin@yildiz.edu.tr

Abstract

Traditional simulators predominantly operate with position control at specific frequencies and largely neglect the appropriate imposition of accelerations on the structure. This restricts the application of realistic accelerations during fatigue testing and reduces the fidelity of tests to real road conditions. This study proposes an integrated experimental–analytical framework for motorcycle testing under laboratory conditions. Within the framework, smooth displacement reference signals are generated from noisy field-measured acceleration signals through Fourier-based harmonic curve fitting and analytic integration. Subsequently, a nonlinear adaptive backstepping control algorithm is designed to ensure accurate replication of these references within the 0–25 Hz bandwidth under parametric uncertainties. This approach provides a valuable and repeatable alternative to conventional on-road testing, ensuring that realistic road-induced accelerations are accurately imposed on the motorcycle structure during fatigue testing. Experimental signals were collected from a motorcycle on three different road surfaces, and the performance of the generated reference signals was evaluated in both the time and frequency domains. Experiments conducted on a real-time industrial controller demonstrated that the proposed controller exhibits superior tracking performance across all road profiles, achieving a Root Mean Square Error (RMSE) as low as 1.3 mm, while the Fourier-based reconstruction achieves R^2 values approaching 0.97. The controller maintains consistent precision and negligible performance variance despite significant differences in road characteristics, thereby offering a controlled and cost-effective laboratory simulation alternative to conventional on-road durability testing.

Keywords: road simulation; Fourier curve fitting; adaptive backstepping control; motorcycle dynamics; hydraulic actuator

Check for updates

Academic Editor: Xianxu 'Frank' Bai

Received: 6 March 2026
Revised: 4 April 2026
Accepted: 14 April 2026
Published: 16 April 2026

Copyright: © 2026 by the authors. Licensee MDPI, Basel, Switzerland. This article is an open access article distributed under the terms and conditions of the Creative Commons Attribution (CC BY) license.

1. Introduction

The rapid evolution of the automotive industry demands careful validation of vehicle durability, ride comfort, and safety standards. The industry is significantly shifting its focus from time-consuming proving ground tests to laboratory-based road test rigs. Hydraulic road test rigs have emerged as a key component of this validation process. These test

rigs offer the critical ability to replicate complex road-vehicle interactions in a repeatable and controlled environment. However, achieving high-fidelity reproduction of real-world dynamics within a test rig remains a formidable engineering challenge. This is primarily due to the nonlinearities of hydraulic actuators and the difficulty of generating accurate reference signals from field-measured acceleration data, which inherently contain noise, making the transformation to displacement trajectories challenging. Traditional signal processing methods often fail to preserve the primary characteristics of the road profile, resulting in differences between the road and the test rig. Furthermore, even with a perfect reference signal, standard controllers often struggle to maintain tracking precision against the parametric uncertainties of hydraulic systems. Motivated by these limitations, this study introduces a unified experimental–analytical framework. By integrating Fourier-based curve fitting with a nonlinear adaptive control strategy, this research aims to provide a robust methodology for high-fidelity motorcycle durability testing.

A significant body of research has focused on virtual simulation models of motorcycle and bicycle dynamics. He et al. [1] developed a comprehensive multi-degree-of-freedom model that incorporates steering geometry, tire slip dynamics, frame flexibility, and rider inputs; their work particularly enables realistic roll–steer behavior in interactive riding simulations. Shoman and Imine [2] systematically improved model accuracy by comparing simulation results with data collected from a physical bicycle prototype, thereby enhancing the dynamic consistency and educational potential of riding simulators. Owczarkowski et al. [3] analyzed the tipping dynamics of bicycles in detail within an LQR-based stabilization framework and examined the influence of controller design on stability across different speed conditions. Zhao et al. [4] experimentally and numerically investigated the effects of rider biomechanics on system response in suspension-equipped cycling trainers, providing detailed insight into the role of human–bicycle interaction in vertical vibration performance. Since earlier research has primarily relied on synthetic or simplified excitations, there is a clear need to validate hydraulic systems with real-world reference signals. Motivated by this necessity, the present study focuses on high-fidelity reconstruction of real road signals, establishing a wide dataset through comprehensive motorcycle experiments on the road.

Another major direction in the literature concerns the estimation of road profiles or vehicle parameters based on onboard measurements. Deep learning-based reconstruction methods [5], sliding-mode observers and optimization techniques for bicycle parameter identification [6,7], and sensor-fusion-based estimation strategies such as the adaptive Kalman filtering framework of Arat et al. [8] demonstrate strong capabilities for inferring road disturbances and suspension states. Similar studies estimate road roughness characteristics [9], while Yao et al. [10] propose UKF-based harmonic identification techniques. These contributions provide valuable bases for signal estimation. In the proposed framework, Fourier-based curve fitting is adopted over alternative signal processing methods due to several practical advantages for offline reference signal generation. Fourier-based harmonic decomposition has been widely employed in road profile characterization, owing to its ability to efficiently represent broadband excitations as a superposition of sinusoidal components [11,12]. Unlike direct numerical double integration, which amplifies low-frequency noise components and introduces positional drift that grows with integration time [13], the Fourier-based approach performs integration analytically, yielding smooth, drift-free displacement trajectories. In comparison, wavelet-based methods, while offering superior time-frequency localization for detecting localized road anomalies [11], require careful selection of the mother wavelet and decomposition level, introducing additional tuning complexity that is unnecessary for the offline periodic reference signal generation targeted in this study. Polynomial fitting, on the other hand, is prone to Runge's phenomenon at

higher orders and does not naturally support frequency-domain characterization of road-induced periodic excitations, making it less suitable for the broadband signal representation required in this study.

Parallel to the advancements in signal reproduction, the design of control architectures constitutes the other fundamental pillar for system analysis. Active and semi-active suspension control research offers yet another relevant domain. Time-delay feedback control [14], sliding-mode control with extended state definitions [15], nonlinear adaptive schemes [16], and reinforcement-learning-based semi-active control validated through road testing [17] have all demonstrated significant improvements in vibration mitigation. Kararsiz et al. [18] introduced an adaptive control framework combined with disturbance observers to compensate for unknown road inputs, while Paksoy and Metin [19] proposed a nonlinear semi-active adaptive vibration control strategy validated via HIL experiments on a half-vehicle model. The literature most closely related to the present work focuses on hydraulic road simulators and shaking tables. Chindamo et al. proposed a motorcycle road simulator architecture [20] and demonstrated four-poster reproduction of road profiles for durability testing [21]. Azizi et al. [22] designed and experimentally evaluated an electro-hydraulic road-excitation simulator, while Shen et al. [23] introduced feed-forward inverse control for transient waveform replication. Metin et al. [24] demonstrated that their proposed controller enables the hydraulic cylinder to track reference road inputs more accurately, particularly by effectively suppressing the nonlinear effects arising from pressure dynamics and load variations through the backstepping structure. However, the framework of Chindamo et al. [20,21] relies on direct signal replay without adaptive compensation for hydraulic parametric uncertainties, nor does it address the noise-induced drift problem in acceleration-to-displacement conversion. Metin et al. [24] assume that the displacement reference signal is directly available, whereas in practice field-measured acceleration data contain noise that renders direct double integration unreliable. The present study addresses both gaps simultaneously: Fourier-based harmonic fitting converts noisy acceleration measurements into smooth, drift-free displacement trajectories via analytic integration, and an adaptive backstepping controller compensates for real-time parametric uncertainties in the hydraulic actuator. Beyond signal fidelity, the proposed framework is specifically designed to replicate the acceleration effects experienced by the motorcycle structure—a critical factor in fatigue analysis of mechanical systems such as automotive suspensions, railway bogies, and aerospace structures. By transforming noisy acceleration signals into smooth displacement references, the framework ensures that the same road-induced acceleration effects are reliably reproduced on the motorcycle under laboratory conditions, distinguishing this work from existing road simulator approaches. Dursun and Bayram [25] presented a model-based iterative learning control (ILC) strategy—where repeated execution of the same trajectory enables cycle-to-cycle improvement in tracking accuracy. In addition, modeling and control of hydraulic test systems have been addressed in the literature. Taşağıl et al. [26] presented modeling and parametric analysis of elastomer material test systems, while Taşağıl et al. [27] implemented adaptive fuzzy PID control on a hydraulically driven axle shaft test system. These studies highlight the importance of adaptive control strategies in hydraulic test rigs operating under varying load conditions and parameter uncertainties. Consequently, tracking performance in hydraulic systems arises from the interaction between the supply pressure, the servo-valve dynamics, and the external load forces. Nonlinearities significantly influence the control precision of the system. The integration of adaptive control mechanisms can further improve tracking behavior by compensating for parametric uncertainties and varying operating conditions. The high control performance of adaptive algorithms in nonlinear systems has led researchers to extend their use in systems requiring multi-physics modeling, such as hydraulic road simulators.

The significance of accurate reference reproduction in road simulation, combined with the demonstrated tracking capability of adaptive control algorithms for hydraulic systems, underscores the necessity of a unified testing framework. In contrast to traditional road simulators that utilize position control at fixed frequencies without explicitly considering the acceleration effects on the structure, this study introduces a framework for the replication of road-induced accelerations on the motorcycle structure. To succeed in this framework's aim, a practical position-controlled approach is developed that reliably reproduces real-road acceleration effects within the 0–25 Hz operational bandwidth—the frequency range governing motorcycle suspension dynamics and structural fatigue. The novelty of this work can be summarized as follows:

- By employing a Fourier-based curve fitting method, the proposed framework enables the transformation of noisy acceleration data into smooth, differentiable displacement trajectories. This significantly enhances the quality of the reference signal available for the control system.
- Beyond signal processing, the proposed methodology implements an adaptive control law that estimates hydraulic parameters in real-time. This provides a more accurate representation of the system dynamics under varying road loads, directly enhancing the performance of the test rig in reproducing real-world vibrations within the targeted frequency bandwidth.
- The framework enables rigorous motorcycle durability testing in a laboratory environment by ensuring road-induced acceleration effects. The proposed framework is applicable to structural fatigue testing in automotive suspensions, railway bogies, and aerospace structures.

Consequently, the present study proposes a comprehensive experimental–analytical framework for reproducing real-road motorcycle vertical dynamics in laboratory conditions. Acceleration data were collected on three road surfaces—smooth asphalt, cobblestone, and pavement stones—while towing the motorcycle to eliminate engine-induced vibration. The measured vertical accelerations were harmonically reconstructed via curve fitting and transformed to displacement reference signals. These trajectories were then applied to a vertically actuated hydraulic cylinder controlled by a nonlinear adaptive backstepping algorithm developed for a motorcycle. The adaptive laws updated uncertain hydraulic parameters associated with effective bulk modulus, flow–pressure characteristics, and other unmodeled dynamic effects. Experiments conducted on a 1-kHz real-time industrial controller demonstrated that the proposed framework successfully reproduces the dominant features of real-road motorcycle accelerations across all tested surfaces.

2. Methodology

The workflow of the study consists of four main stages: data acquisition, signal processing, test system design, and control algorithm development. First, acceleration data were collected from a motorcycle driven within the campus of Yildiz Technical University, Istanbul. In this stage, an accelerometer was integrated into the motorcycle to measure real road-induced vibrations during riding. The general structure of the proposed methodology is shown in Figure 1. After data acquisition, the aim was to obtain the displacement motion of the hydraulic pistons in the laboratory test rig. To achieve this, the measured acceleration signal was transformed into a displacement reference signal. The transformation was performed by fitting the acceleration data using Fourier-based harmonic curve fitting. After that, the fitted acceleration signals were converted to obtain the equivalent displacement profile. This displacement signal was used as the reference trajectory for the hydraulic piston system. The test rig was designed to drive a full-scale motorcycle using two hydraulic pistons mounted at the front and rear ends. After establishing a safe

and stable operating procedure, the motorcycle was securely fixed to the test platform. The proposed control algorithm implemented on the rig was an adaptive control strategy, developed to compensate for uncertainties in the hydraulic-piston system parameters. A detailed analysis of each component of the study is presented in the subsequent sections.

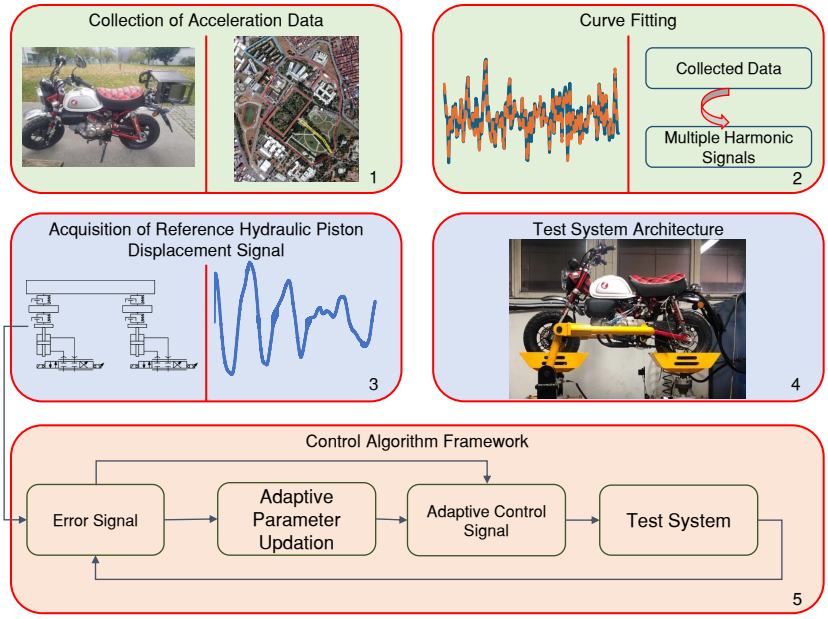


Figure 1. The workflow of the study: (1) collection of acceleration data, (2) curve fitting, (3) acquisition of reference hydraulic piston displacement signal, (4) test system architecture, and (5) control algorithm framework.

2.1. Data Acquisition

This section describes the field data acquisition procedure used to generate the hydraulic-piston reference signals for the laboratory test system. The test system is designed for motorcycle fatigue and endurance testing. Data collection was carried out on 11 November 2024 at Yildiz Technical University's Davutpasa Campus, Istanbul. During the data collection, the acceleration data were collected from a Honda Monkey model motorcycle on three different road surfaces: asphalt, paving stones, and cobblestones, at varying motorcycle velocities.To isolate road-induced vibrations and exclude engine-generated disturbances, the motorcycle engine was not ridden during the measurements; instead, the motorcycle was towed by an external vehicle via a tow rope. The test area can be seen in Figure 2.

In the test area,

- Red marked road: Asphalt Road;
- Blue marked road: Paving Stones;
- Yellow marked road: Cobblestones.

The measurement system components and their specifications are summarized in Table 1. A A Sirius HD-STGS/Module A (Dewesoft d.o.o., Trbovlje, Slovenia) data acquisition unit was used for synchronized data logging, while a Dewesoft IMU provided GPS-based vehicle speed and position information. Vertical acceleration at the motorcycle chassis was measured using a Kistler 8396A010ATTA00 MEMS triaxial accelerometer with a ± 10 g range, 400 mV/g sensitivity, and $\pm 0.3\%$ FSO linearity, mounted the center of mass with adhesive attachment to minimize measurement artifacts. Acceleration data were sampled at 1000 Hz, and a 0–25 Hz low-pass filter was subsequently applied in post-processing to retain only the road-induced low-frequency content that is relevant to

motorcycle suspension dynamics, in accordance with the operational bandwidth of the test rig. During the measurements, the motorcycle speed was selected in accordance with the traffic rules for the road used. There were also numerous speed bumps on the selected route. Thus, road-induced impact effects on the motorcycle were also captured in the tests.



Figure 2. Overview of the data acquisition system and test track: (**a**) the test area in Yildiz Technical University, where the red line indicates the asphalt road, the blue line indicates the paving stones, and the yellow line indicates the cobblestones, (**b**) the motorcycle equipped with the measurement unit (highlighted with red box), (**c**) close-up view of the acceleration sensor placement (highlighted with red box).

Table 1. Specifications of the acceleration data acquisition system.

Component	Model	Key Specifications
Accelerometer	Kistler 8396A010ATTA00	MEMS triaxial; ±10 g; 400 mV/g; 0–2000 Hz; 1000 Hz sampling; ±0.3% FSO
Data Acquisition Unit	Sirius HD-STGS/ Module A	Data logging and synchronization
IMU 1	Dewesoft	GPS-based motorcycle speed measurement and positioning

2.2. Curve Fitting

The accurate representation of road-induced excitations is essential for reproducing realistic dynamic responses, especially for the analysis of the fatigue effect on the vehicles in the laboratory environment. The acceleration signals collected from the motorcycle were used to reconstruct the equivalent displacement trajectories since the direct measurement of the road displacement profile is often impractical in on-road experiments. This reconstruction serves as the base for developing the reference signal of the hydraulic pistons in the test rig. Thus, the experimentally acquired acceleration signals were transformed into displacement signals of the pistons that excite the motorcycle in the industrial application. For this transformation, a Fourier-based curve-fitting approach that is given in Equation (1) was employed, assuming that the acceleration response induced by road irregularities can be expressed as a superposition of harmonic components. This assumption is widely accepted

in road surface modeling and enables an efficient frequency-domain characterization of the measured data.

In the curve fitting analysis, three different road acceleration signals (asphalt, paving, and cobblestones) were investigated. The number of harmonic components was determined empirically by evaluating the fitting performance metrics defined in (3)–(5) on the measured acceleration signals. Starting from a small number of components, harmonics were progressively added until the coefficient of determination R^2 exceeded 0.94 for all three road surfaces, beyond which additional components produced negligible improvement in the fitting accuracy. This process yielded 144 harmonic components distributed across 72 distinct frequencies spanning the 0–25 Hz range, which corresponds to the operational bandwidth of the MOOG D661-6487C servo valve (Moog Inc., East Aurora, NY, USA) and encompasses the primary frequency content of motorcycle suspension dynamics. The exclusion of frequency content above 25 Hz is further justified by the attenuation characteristics of the motorcycle suspension system, which acts as a low-pass filter for road-induced excitations. Each harmonic signal was characterized by its amplitude and frequency, providing a detailed frequency-domain representation of the road-induced excitation. Consequently, the fitted profiles closely replicated the experimentally measured acceleration data, as presented in Table 2. The coefficient of determination (R^2) approached unity, indicating an ideal fit, while both the root mean square error (RMSE) and mean absolute error (MAE) values were found to be low. The mathematical representation of the performance indices is given between Equations (3) and (5). An illustration between the measured and reconstructed signals, shown in Figure 3, confirms the strong correlation and demonstrates that the fitted curve accurately captures both the periodic and transient characteristics of the measured acceleration data. The amplitude spectrum of the harmonic components is illustrated in Figure 4. The high agreement between the experimental and fitted responses validates the effectiveness of the Fourier-based harmonic decomposition approach for generating representative road excitation profiles. This process forms the foundation for the dynamic analysis and control algorithm testing performed in the subsequent sections under realistic excitation conditions.

$$a(t) \approx \sum_{i=1}^{n} (A_i cos(2\pi f_i t) + B_i sin(2\pi f_i t)) \tag{1}$$

The displacement reference signal was obtained analytically from the fitted harmonic coefficients $\{A_i, B_i, f_i\}$. The constant term produced by the fitting procedure was excluded from the reconstruction to prevent quadratic growth in the integrated displacement, which would be physically unrealistic and incompatible with the actuator stroke limit. For each harmonic component, the corresponding displacement was obtained by dividing the acceleration amplitude by $(2\pi f_i)^2$, yielding:

$$x(t) = \sum_{i=1}^{72} \left[-\frac{A_i}{(2\pi f_i)^2} \cos(2\pi f_i t) - \frac{B_i}{(2\pi f_i)^2} \sin(2\pi f_i t) \right] \tag{2}$$

This analytic procedure eliminates the noise amplification inherent in numerical double integration, resulting in smooth, drift-free displacement trajectories verified to remain within the actuator stroke limit. The resulting reference piston signals are illustrated in Figure 4.

$$\text{RMSE} = \sqrt{\frac{1}{N} \sum_{i=1}^{N} (a_i - \hat{a}_i)^2} \tag{3}$$

$$\text{MAE} = \frac{1}{N}\sum_{i=1}^{N}|a_i - \hat{a}_i| \tag{4}$$

$$R^2 = 1 - \frac{S_{res}}{S_{tot}} = 1 - \frac{\sum_{i=1}^{N}(a_i - \hat{a}_i)^2}{\sum_{i=1}^{N}(a_i - \bar{a})^2} \tag{5}$$

In these equations, N denotes the total number of data points, while a_i and $\hat{a}_i$ represent the actual measured acceleration values and the predicted values, respectively. Additionally, $\bar{a}$ indicates the mean of the actual measurements, S_{res} corresponds to the residual sum of squares, and S_{tot} represents the total sum of squares. A and B are the coefficients of the harmonic signals, f is the frequency, and t represents time.

Table 2. Performance evaluation of the curve-fitting algorithm.

Road Type	R^2	RMSE	MAE
Cobblestones	0.9694	8.8184	7.5211
Paving Stones	0.9451	11.8205	9.8296
Asphalt Road	0.9719	7.9879	6.9220

In Figure 4c, the reference piston signal derived from the acceleration signal can be seen. After identifying the reference signal for the control algorithm, the error signal is created from the reference signal and the system feedback signal during the control signal design. In the next section, the design of the control algorithm is presented.

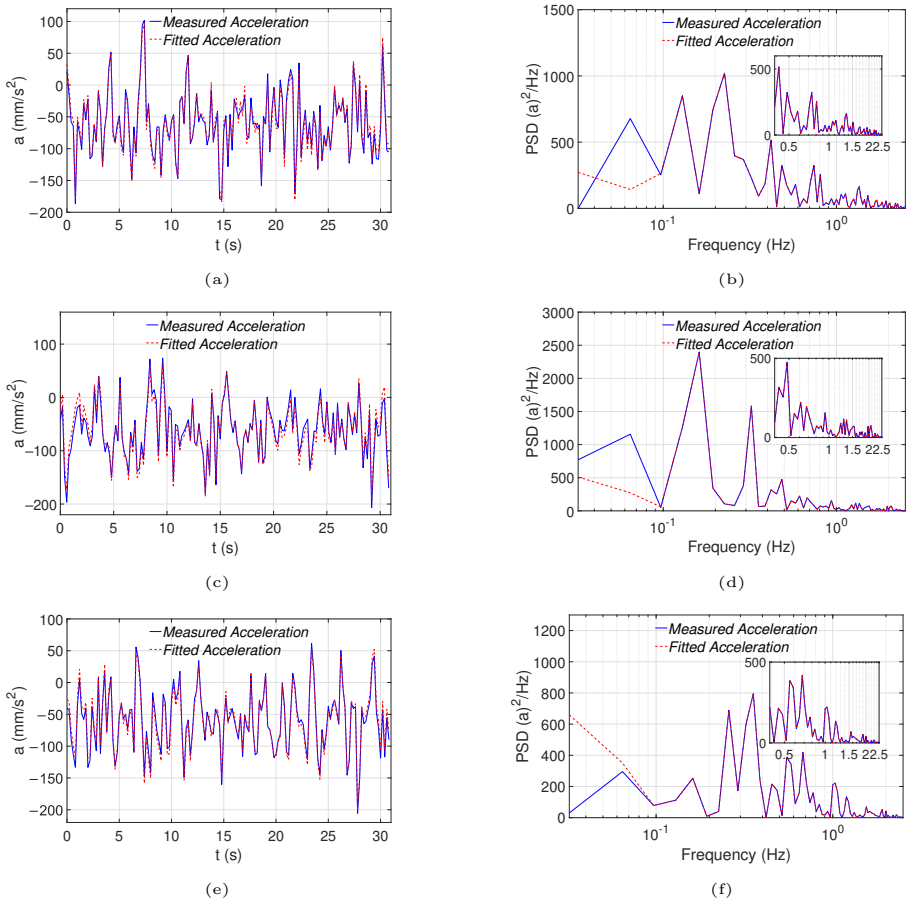


Figure 3. The filtered and the fitted signal comparison, (**a**) Cobblestones time domain, (**b**) Cobblestones frequency domain, (**c**) Paving stones time domain, (**d**) Paving stones frequency domain, (**e**) Asphalt road time domain, (**f**) Asphalt road frequency domain.

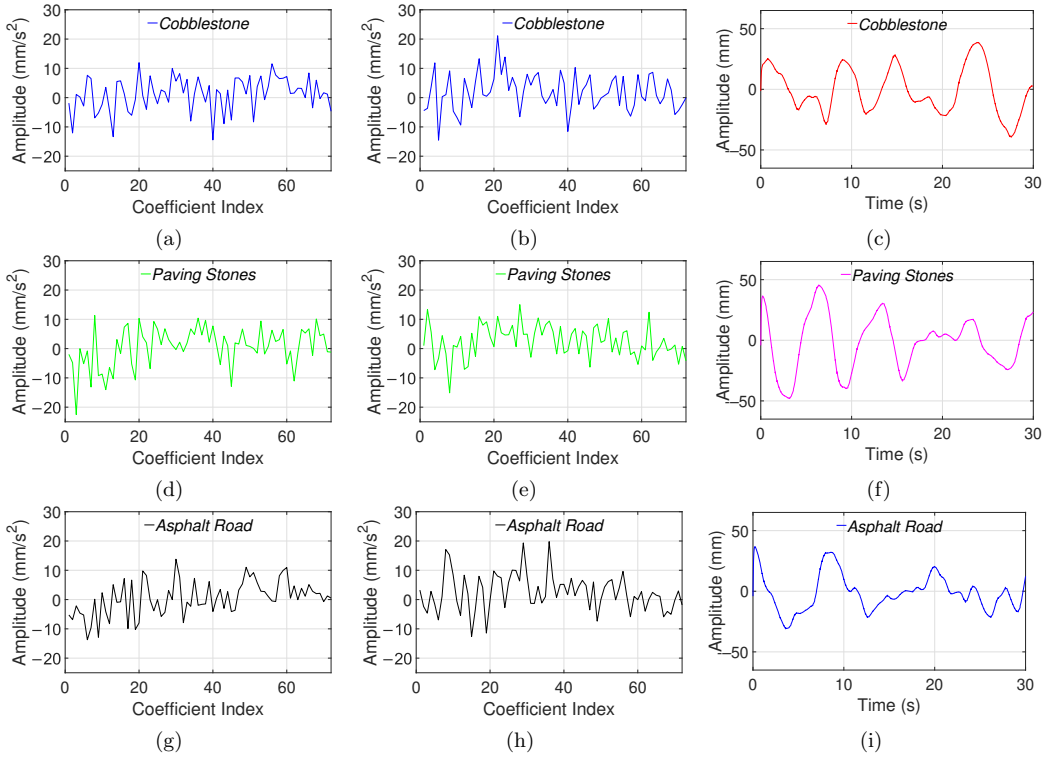


Figure 4. Analysis of the fitted harmonic signal components and the reference trajectory: (**a**,**d**,**g**) cosine coefficients of the fitted harmonic signal, (**b**,**e**,**h**) sine coefficients of the fitted harmonic signal (**c**,**f**,**i**) the reference piston signal.

2.3. Adaptive Control Design

In this section, the adaptive control algorithm design for the trajectory tracking control of the hydraulic piston systems is presented. The illustration of the hydraulic piston system is shown in Figure 5 and the parameter list can be seen in Table 3.

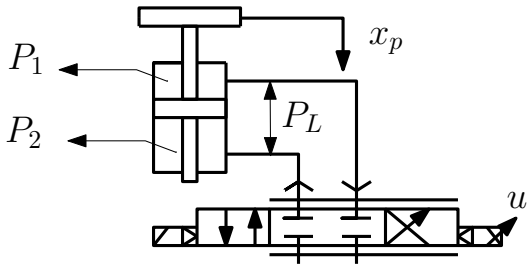


Figure 5. The physical representation of the hydraulic piston system.

In the hydraulic system, the valve command signal is designed as the control input of the system that controls the hydraulic actuator response by generating a pressure difference between the upper and lower chambers of the hydraulic piston. This pressure differential, denoted by $P_L(P_L = P_1 - P_2)$ as shown in Figure 5, varies as a function of time and directly determines the vertical displacement of the piston rod. Consequently, the controlled motion of the hydraulic piston induces vertical vibrations on the motorcycle structure mounted on the test platform, thereby replicating the real road-induced excitation under laboratory conditions. The mathematical model of the hydraulic system, corresponding to the physical configuration shown in Figure 5, is defined between Equations (6) and (7).

$$m_p \ddot{x}_p = A_p P_L \tag{6}$$

$$\dot{P}_L = f_1 \dot{x}_p + f_2 P_L + f_3 \sqrt{P_s - sign(u) P_L} u \tag{7}$$

$$\begin{aligned} f_1 &= -\frac{4\beta A_p}{V} \\ f_2 &= -\frac{4\beta C_t l}{V} \\ f_3 &= \frac{4\beta C_d w k_i}{V\sqrt{\rho}} \end{aligned} \tag{8}$$

where m_p is the piston mass; x_p is piston displacement; $\dot{x}_p$,$\ddot{x}_p$ are piston velocity and acceleration, respectively; A_p is the piston effective area; P_L is the valve-related pressure differential state; $\dot{P}_L$ is the time derivative of P_L; u is the valve command input; P_s is the supply pressure; $sign(u)$ is the signum function of u; β is the fluid bulk modulus; V is the hydraulic control volume; C_t is the leakage conductance; C_d is the discharge coefficient; w is the valve spool gradient; k_i is the electrical gain; ρ is the fluid density; f_1, f_2, and f_3 are coefficients defined in Equation (8). The parameters f_1, f_2, and f_3 in Equation (8) are treated as adaptive parameters. These parameters were selected as the uncertain parameters in the hydraulic piston system due to handling parametric uncertainties, such as variations in the effective bulk modulus (β) resulting from temperature changes. The adaptation parameter f_1 represents the hydraulic stiffness term relating to the piston velocity dynamics, f_2 characterizes the total leakage coefficient (C_{tl}) of the system, and f_3 represents the control input gain (control effectiveness), which is directly influenced by the discharge coefficient (C_d) and the valve spool gradient (w).

Table 3. Parameter table.

Symbol	Definition	Unit	Value
m_p	Piston Mass	kg	4
A_p	Piston Area	m^2	256.4×10^{-5}
P_1, P_2	Cylinder Internal Pressures	bar	-
P_s	Supply Pressure	bar	210
x_p	Piston Position	m	-
$\dot{x}_p$	Piston Velocity	m/s	-
P_L	Pressure Difference	bar	-
ρ	Hydraulic Oil Density	kg/m^3	850
β	Oil Bulk Modulus	N/m^2	1.4×10^9
C_{tl}	Leakage Coefficient	$\frac{m^3}{s \cdot Pa}$	1.3324×10^{-16}
C_d	Discharge Coefficient	-	0.62
ω	Servo Valve Area Gradient	m	0.024
V_t	Total Cylinder Volume	m^3	320.5×10^{-6}
k_i	Electrical Gain	m/A	3.0×10^{-4}
k_1, k_2, k_3	Control Gains	-	9800, 5000, 3600
$\Gamma_{1,2,3}$	Adaptation Gains	-	700, 700, 700

To quantify the control objective, the tracking error signal was defined as Equation (9)

$$e(t) = x_r(t) - x_p(t) \tag{9}$$

where $e(t)$ is the scalar error signal between the reference piston displacement signal and the piston displacement signal. The candidate Lyapunov function can be defined as Equation (10) to investigate the stability analysis of the system

$$\begin{aligned} V(t) &= \frac{1}{2}e^2(t) + \frac{1}{2}z_1^2(t) + \frac{1}{2}z_2^2(t) \\ &+ \frac{1}{2}\tilde{f}_1\Gamma_{f_1}\tilde{f}_1 + \frac{1}{2}\tilde{f}_2\Gamma_{f_2}\tilde{f}_2 + \frac{1}{2}\tilde{f}_3\Gamma_{f_3}\tilde{f}_3 \end{aligned} \tag{10}$$

where $z_1(t)$ and $z_2(t)$ represent the intermediate state between the virtual control signals (ϕ_1, ϕ_2) and the system states (x_p,P_L). The notation $(\hat{\bullet})$ denotes the estimated value of a variable $(\bullet)$, while the estimation error between the actual and estimated parameters is defined as $(\tilde{\bullet}) = (\bullet) - (\hat{\bullet})$. The intermediate state can be found in Equations (11) and (12).

$$z_1(t) = \phi_1 - \dot{x}_p \tag{11}$$

$$z_2(t) = \phi_2 - P_L \tag{12}$$

where the virtual control signals ϕ_1 and ϕ_2 are introduced as part of the back-stepping design to facilitate the derivation of the actual control input. The time derivative of the virtual control signal in Equations (13) and (14) are incorporated into the derivation of Equation (10).

$$\phi_1 = (\dot{x}_r + k_1 e) \tag{13}$$

$$\phi_2 = \frac{m_p}{A_p}\left(k_2 z_1 + e + \ddot{x}_r + k_1\left(\dot{x}_r - \dot{x}_p\right)\right) \tag{14}$$

Accordingly, the time derivative of the candidate Lyapunov function is obtained as in Equation (15)

$$\begin{aligned} \dot{V} &= e(-k_1 e + z_1) + z_1\left(-k_2 z_1 - e + \frac{A_p}{m_p}z_2\right) \\ &+ z_2\left[\frac{m_p}{A_p}\left(k_2\left((\ddot{x}_r + k_1(\dot{x}_r - \dot{x}_p)\right) - \frac{A_p}{m_p}P_L\right)\right. \\ &\left. + \dot{e} + \dddot{x}_r + k_1\left(\ddot{x}_r - \frac{A_p}{m_p}P_L\right)\right) - \dot{P}_L\Bigg] \\ &+ \tilde{f}_1\Gamma_{f_1}(-\dot{\hat{f}}_1) + \tilde{f}_2\Gamma_{f_2}(-\dot{\hat{f}}_2) + \tilde{f}_3\Gamma_{f_3}(-\dot{\hat{f}}_3) \end{aligned} \tag{15}$$

The proposed control algorithm is formulated as shown in Equation (16)

$$\begin{aligned} u = \frac{1}{\hat{f}_3\sqrt{P_s - \mathrm{sign}(u)P_L}}\Bigg[&\frac{m_p}{A_p}\left(k_2\left(\ddot{x}_r + k_1(\dot{x}_r - \dot{x}_p)\right.\right. \\ &\left.\left. - \frac{A_p}{m_p}P_L\right) + \dot{e} + \dddot{x}_r + k_1\left(\ddot{x}_r - \frac{A_p}{m_p}P_L\right)\right) \\ &- \hat{f}_1\dot{x}_p - \hat{f}_2 P_L + k_3 z_2 + \frac{A_p}{m_p}z_1\Bigg] \end{aligned} \tag{16}$$

where k_1, k_2 and k_3 are the user-defined positive control gains. The control gains k_1, k_2, k_3 and the adaptation gains Γ_1, Γ_2, Γ_3 were selected to satisfy the stability conditions established by the Lyapunov analysis and to regulate the convergence rate of the adaptive

parameter update laws. To prevent numerical singularity in the control law (16) and a sign change at the f_3, a lower-bound constraint is enforced on the adaptive estimate $\hat{f}_3$ throughout the experiment, ensuring that $\hat{f}_3(t) \geq f_{3,\min} > 0$ for all $t \geq 0$, which is physically consistent with the definition $f_3 = 4\beta C_d w k_i / (V\sqrt{\rho}) > 0$, as confirmed by the experimental results. The adaptation laws for the estimated parameters can be found in Equation (17)

$$\begin{aligned} \dot{\hat{f}}_1 &= -\Gamma_{f_1} \dot{x}_p z_2 \\ \dot{\hat{f}}_2 &= -\Gamma_{f_2} P_L z_2 \\ \dot{\hat{f}}_3 &= -\Gamma_{f_3} \sqrt{P_s - sign(u) P_L} u z_2 \end{aligned} \tag{17}$$

When the control gains k_1, k_2 and k_3 are appropriately selected, the end of the stability analysis can be expressed as

$$\dot{V} = -k_1 ||e||^2 - k_2 ||z_1||^2 - k_3 ||z_2||^2 \tag{18}$$

From the candidate Lyapunov function $V(t)$ in Equation (10) and its time derivative $\dot{V}(t)$ in Equation (18), it follows that $V(t) \in \mathcal{L}_\infty$. Consequently, the signals $e(t)$, $z_1(t)$, $z_2(t)$, $\tilde{f}_1$, $\tilde{f}_2$, $\tilde{f}_3 \in \mathcal{L}_\infty$. Furthermore, from the closed-loop dynamics, $\dot{e}(t)$ is bounded since all signals remain in $\mathcal{L}_\infty$. By Barbalat's Lemma [28], it follows that:

$$\lim_{t \to \infty} e(t) = 0 \tag{19}$$

The expanded stability analysis is provided in Appendix A.

2.4. Experimental Setup

In this section, the experimental framework established to validate the proposed adaptive control algorithm is presented. First, field measurements were conducted to capture the vertical acceleration response of the motorcycle on various road terrains, serving as the basis for the curve-fitted reference signals described in the previous section. Subsequently, a custom-designed motorcycle hydraulic test rig was utilized to reproduce these road profiles under controlled conditions. The detailed specifications of the mechanical configuration, the hydraulic actuation system, and the data acquisition infrastructure are provided in the following subsections.

2.4.1. Mechanical Configuration and Hydraulic Actuation

The experimental framework developed for this study is configured as a dual-actuator motorcycle test system, designed to validate the effectiveness of adaptive control algorithms under laboratory conditions. This setup allows for the independent control of the front and rear wheel displacements. The configuration is designed to reproduce driving scenarios accurately by exposing the motorcycle tires to vertical excitations that mimic real-world road profiles. The 100 ms inter-actuator delay applied between the front and rear actuators was determined based on the Honda Monkey wheelbase distance ($L \approx 1.2$ m) and the average test speed of 43.2 km/h (12 m/s), yielding $t_{delay} = L/v = 1.2/12 \approx 100$ ms. This value represents the time required for a road irregularity to travel from the front to the rear wheel contact patch at the nominal operating condition. The setup was built on high-rigidity steel construction. The actuation system utilizes two custom-manufactured hydraulic cylinders with a piston diameter of ∅80 mm, a rod diameter of ∅56 mm, and a maximum stroke length of 125 mm. These cylinders are positioned to transfer vertical motion directly to the contact patches of the motorcycle tires. To maintain kinematic stability and prevent the vehicle from tipping during dynamic testing, lateral stabilizer arms were integrated into the frame. These arms provide a kinematic constraint that permits free

vertical translation (heave and pitch motion) while rigidly restricting lateral roll and yaw degrees of freedom. To address the nonlinear flow characteristics inherent in hydraulic systems, MOOG D661-6487C high-performance servo valves are employed. These valves are critical for enhancing the system's dynamic response, enabling high-fidelity tracking of road inputs within the low-to-medium frequency range (0–25 Hz), which corresponds to the primary bandwidth of vehicle suspension dynamics.

2.4.2. Control Architecture and Data Acquisition

The control infrastructure is built upon the B&R automation architecture, selected for its deterministic real-time processing capabilities. The control algorithms, including the proposed adaptive control law, are embedded in the system within the Automation Studio environment and executed on a B&R APC910 industrial PC (B&R Industrial Automation, Eggelsberg, Austria). This controller manages the exchange of data between the servo valves, integrated linear position sensors, and pressure transmitters via analog and digital input/output modules. The system operates with a closed-loop cycle time of 1 ms to ensure the stability of the adaptive parameters during transient operation. Position feedback is obtained from integrated linear position sensors mounted on the hydraulic cylinders, enabling direct measurement of piston displacement. In addition, a wire-type potentiometric position sensor is used to measure the vertical displacement of the motorcycle body. Pressure measurements are obtained using pressure transmitters, enabling real-time monitoring of hydraulic pressure variations within the system. All sensor signals are synchronously acquired by the APC910 unit, allowing direct comparison between the reference road profile and the measured system response. This synchronized data acquisition enables accurate evaluation of the control performance under realistic dynamic conditions. It should be noted that the performance of the control system is inherently influenced by the physical and operational limitations of the measurement and control hardware. These include sensor measurement ranges, resolution, response times, and actuator input constraints. Therefore, the technical specifications and operational limits of the experimental system components are summarized in Table 4.

Table 4. Specifications of the experimental system components.

Component	Model	Key Specifications
Linear Position Sensor	Novotechnik TH1-0125 (Novotechnik Messwertaufnehmer OHG, Ostfildern, Germany)	Stroke: 125 mm; contactless
Wire Potentiometer	AWP 110-1000-5K (ATEK Electronics Sensor Technologies Inc., Türkiye)	Stroke: 1000 mm; linearity: ±0.25%; 4–20 mA
Pressure Transmitter	SUCO (SUCO Robert Scheuffele GmbH & Co. KG, Fichtenau, Germany)	0–400 bar; 4–20 mA
Servo Valve	MOOG D661-6487C	2-stage electrohydraulic; 350 bar max; 0–25 Hz
Hydraulic Cylinder	∅80/56/125 mm	Bore: 80 mm; rod: 56 mm; stroke: 125 mm; 250 bar max
Industrial Controller	B&R APC910	Real-time; 1 ms cycle; Automation Studio
Analog I/O	B&R modules	Signal I/O; 1000 Hz; ADC limited

3. Results

The experimental investigation was conducted to validate the performance and robustness of the proposed adaptive control algorithm within the hydraulic piston displacement control framework. The control strategy was implemented through an Automation PC (APC), which served as the real-time control unit responsible for implementing the adaptive control algorithm and transferring the control signals to the servo-valve system. During the experimental tests, the control signals drove two hydraulic actuators with a 100-ms delay between the front and rear pistons to generate vertical displacements that imitate the dynamic behavior of different road disturbances. These controlled motions were transmitted to the motorcycle on the test platform, thereby reproducing realistic ride excitations under laboratory conditions. Through the test system, the proposed adaptive control signal was evaluated for maintaining accurate displacement tracking and system stability.

The first experimental validation of the proposed adaptive control scheme was conducted using the Cobblestone road profile, which characterizes a specific variation of road surface irregularities. The corresponding system response is presented in Figure 6. In Figure 6a,b, the tracking performance of the proposed controller scheme at the displacement signals of both the front and rear pistons is superior. Despite the nonlinear dynamics in the system, the tracking error signals between the reference and measured ones remain minimal throughout the duration of the test. Figure 6c,d show the control signals generated by the adaptive control. Furthermore, the effectiveness of the adaptation mechanism is evidenced by the evolution of the estimated parameters shown in Figure 6e–j. The parameters, $\hat{f}_1$, $\hat{f}_2$, and $\hat{f}_3$ representing the hydraulic stiffness, leakage, and control gain, rapidly converge to stable values after an initial transient phase.

In addition to the Cobblestone road profile, the system was investigated by the Paving Stones road profile to evaluate the controller's robust performance under different road conditions. The experimental results for the scenario are illustrated in Figure 7. As shown in Figure 7a,b, the reference trajectory tracking performance at the rear and front cylinders demonstrates superior accuracy. The tracking performance of the proposed controller demonstrates the robustness of the adaptive controller design. The control signals were presented in Figure 7c,d. It can be seen that the front actuator requires a higher magnitude of control input (u) during the initial high-amplitude excitation (especially $0 < t < 1$ s) compared to the rear actuator. Finally, the update of the adaptation parameters was illustrated in Figure 7e–j.

In the last test investigation, the proposed controller algorithm's performance was evaluated under the Asphalt road profile, which represents typical highway driving road conditions. The experimental results are shown in Figure 8. As shown in Figure 8a,b, the designed adaptive controller achieves excellent tracking accuracy. The magnitude of the control signals is presented in Figure 8c,d. The required control voltages are significantly lower than the control input voltages at Cobblestone and Paving stones. The adaptive parameters are presented in Figure 8e–j. These three distinct road profiles with varying characteristics validate the reliability and repeatability of the proposed adaptive control strategy for real-world suspension testing applications. As summarized in Table 5, the numerical metrics confirm the superiority of the proposed framework. The Root Mean Square Error (RMSE) values remain consistently low across varying road profiles, demonstrating the robustness of the control algorithm against different disturbances. Furthermore, the minimal standard deviation of the tracking error indicates high precision and a smooth control response with negligible chattering.

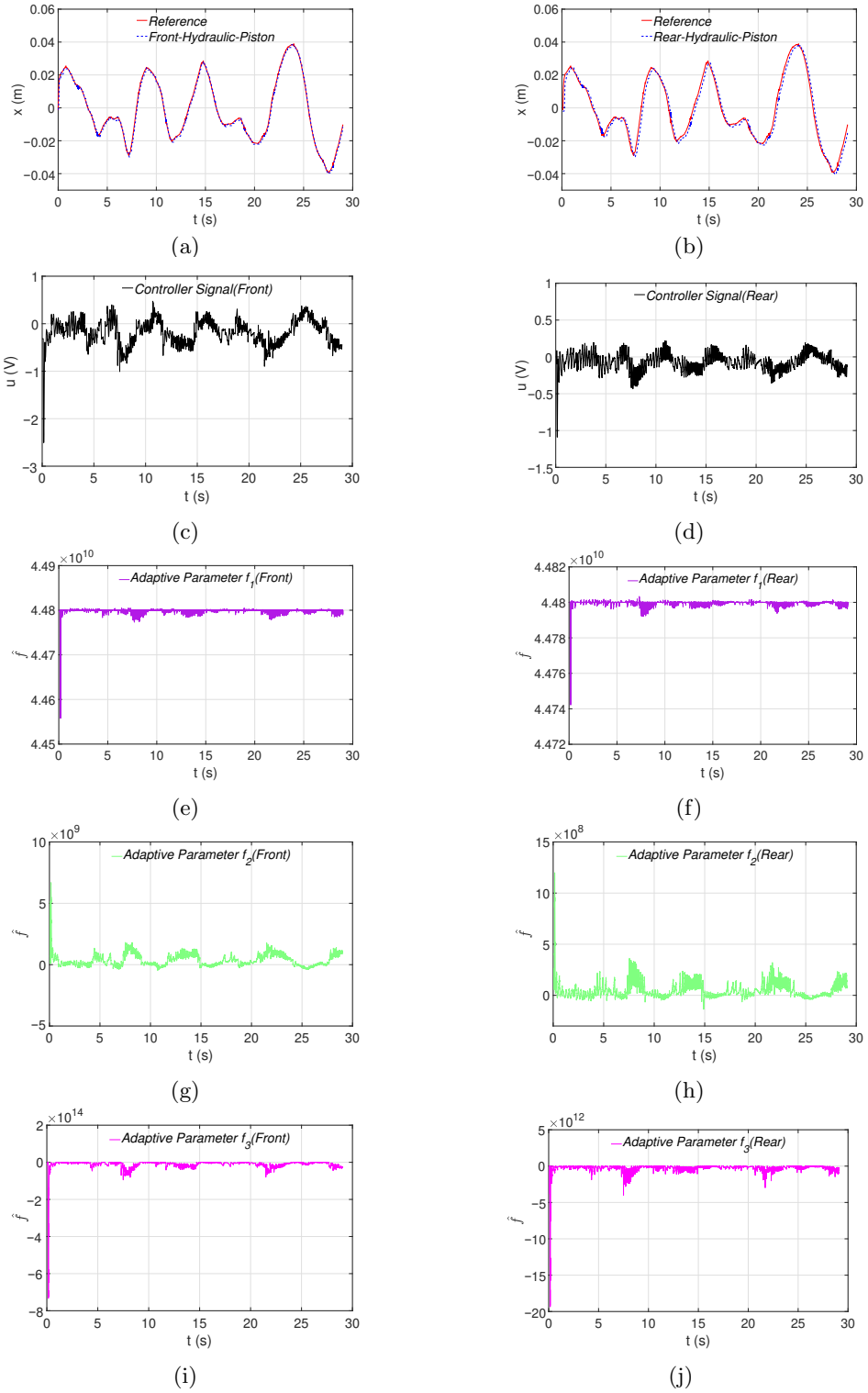


Figure 6. Experimental results of the hydraulic-piston test rig for the Cobblestone road (**a**,**b**) trajectory tracking performance of the front and rear hydraulic pistons compared to the reference displacement signal; (**c**,**d**) control input voltage signals for the front and rear actuators; (**e**–**j**) the update of the adaptive parameters for the front and rear hydraulic pistons $\hat{f}_1$, $\hat{f}_2$, and $\hat{f}_3$.

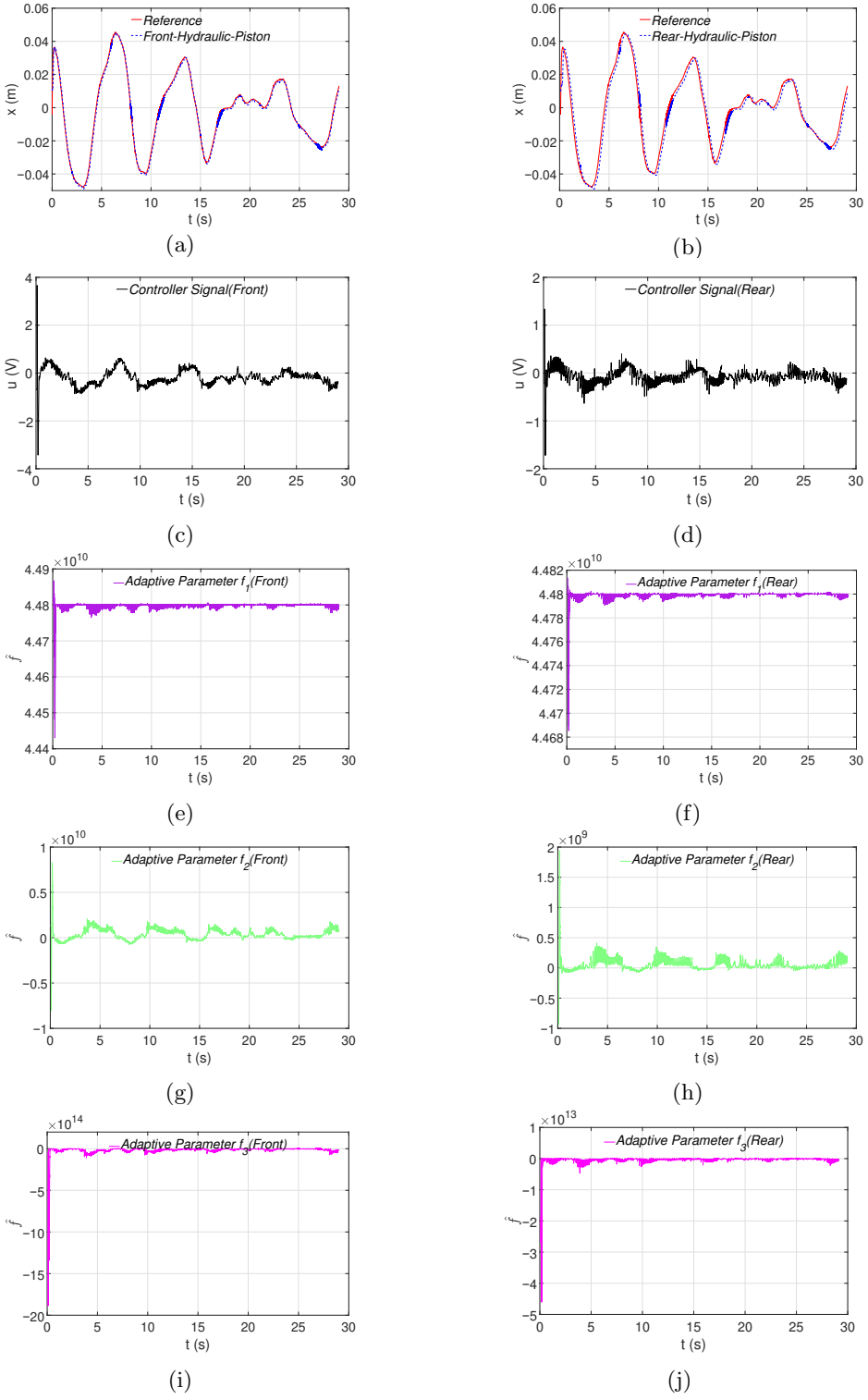


Figure 7. Experimental results of the hydraulic-piston test rig for the Paving Stones road (**a**,**b**) trajectory tracking performance of the front and rear hydraulic pistons compared to the reference displacement signal; (**c**,**d**) control input voltage signals for the front and rear actuators; (**e**–**j**) the update of the adaptive parameters for the front and rear hydraulic pistons $\hat{f}_1$, $\hat{f}_2$, and $\hat{f}_3$.

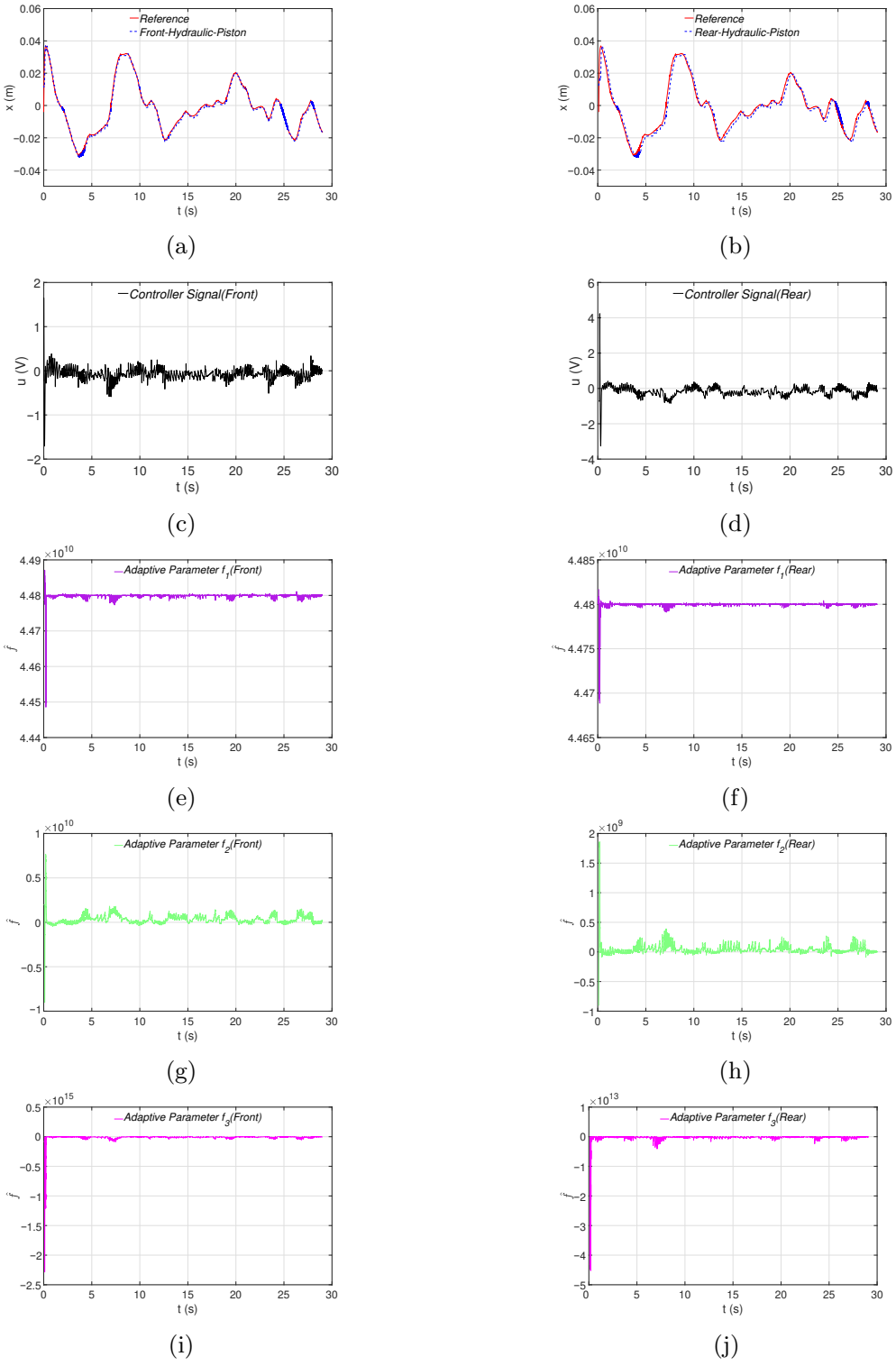


Figure 8. Experimental results of the hydraulic-piston test rig for the asphalt road (**a**,**b**) trajectory tracking performance of the front and rear hydraulic pistons compared to the reference displacement signal; (**c**,**d**) control input voltage signals for the front and rear actuators; (**e**–**j**) the update of the adaptive parameters for the front and rear hydraulic pistons $\hat{f}_1$, $\hat{f}_2$, and $\hat{f}_3$.

Table 5. Performance metrics of the proposed adaptive controller for front and rear suspension systems under three different road profiles.

Road Profile	Location	RMSE (m)	Max. Error ($\|e\|_{max}$)	Std. Dev. ($\sigma(e)$)	Control Effort (u_{rms})
Cobblestone road	Front	0.0013	0.0104	0.0011	0.3159
	Rear	0.0032	0.0199	0.0031	0.1340
Paving Stones road	Front	0.0015	0.0161	0.0014	0.3871
	Rear	0.0041	0.0221	0.0040	0.1609
Asphalt road	Front	0.0013	0.0160	0.0012	0.1440
	Rear	0.0028	0.0208	0.0028	0.3306

The additional investigations in future studies can add to the understanding and applicability of the proposed adaptive control approach in real-world motorcycle testing environments. Directions for future research are summarized below:

- The adaptive control law can be further improved by integrating machine learning-based controllers to improve the adaptation to time-varying road conditions automatically.
- The hydraulic actuation system could be enhanced through the use of high-response servo valves to achieve higher-frequency tracking capability.
- Real-road data acquisition could be expanded to include various weather conditions and loading scenarios to assess the robustness and generalizability of the proposed method.

These extensions can widen the applicability of the proposed framework and contribute to the development of intelligent, high-fidelity motorcycle simulators capable of realistic road signals.

4. Conclusions

This study has successfully established a comprehensive experimental framework for motorcycle testing in a laboratory environment, integrating Fourier-based curve fitting with a nonlinear adaptive backstepping control algorithm. Unlike conventional road simulators that operate with position control without explicitly accounting for the acceleration effects imposed on the structure, the proposed framework targets the reliable replication of road-induced accelerations within the 0–25 Hz bandwidth. By transforming noisy field-measured acceleration signals into smooth, drift-free displacement references via analytic integration, and by compensating for real-time hydraulic parametric uncertainties through adaptive backstepping control, the proposed methodology effectively overcomes the limitations associated with noise in traditional signal reconstruction. Experiments conducted across three different road surfaces demonstrated superior trajectory tracking performance, achieving RMSE as low as 1.3 mm and Fourier-based reconstruction R^2 values approaching 0.97. The controller maintained consistent precision with negligible performance variance across significantly different road characteristics, confirming the robustness of the adaptation mechanism under varying reference road signals. These results collectively demonstrate the practical feasibility of the proposed framework as a repeatable and cost-effective alternative to conventional on-road durability testing. Compared with position-only simulator approaches, the proposed framework critically ensures the appropriate imposition of road-induced accelerations on the motorcycle structure during fatigue testing. The framework significantly reduces test preparation time and logistical costs while maintaining high signal fidelity across different road profile types. Consequently, this framework serves as a reliable and high-fidelity tool for rigorous fatigue analysis and vehicle development, offering a practical laboratory alternative to costly on-road testing.

Author Contributions: Visualization, writing—original draft preparation, investigation, F.C.Y.; methodology, conceptualization, formal analysis, writing—review and editing, supervision, project administration, and data obtaining, M.M.; testing, writing—original draft preparation, and investigation, T.O. All authors have read and agreed to the published version of the manuscript.

Funding: This work was supported by the Scientific and Technological Research Council of Türkiye (TÜBİTAK) under the TEYDEB 1501 program (Project No. 3231321), titled "Development and Verification of a Universal Control Algorithm Capable of Tracking Random Acceleration Values," conducted at Mert Teknik Fabrika Malzemeleri Ticaret ve Sanayi A.Ş.

Institutional Review Board Statement: Not applicable.

Informed Consent Statement: Not applicable.

Data Availability Statement: The data presented in this study are available on request from the corresponding author. The data are not publicly available due to their large volume and the ongoing nature of related research projects.

Acknowledgments: During the preparation of this manuscript, the authors used Gemini 3.1 solely for the purpose of improving the English grammar of sentences. The authors have reviewed and edited the output and take full responsibility for the content of this publication.

Conflicts of Interest: Author Talha Oguz was employed by the company Mert Teknik Fabrika Malzemeleri Ticaret ve Sanayi A.Ş. The remaining authors declare that the research was conducted in the absence of any commercial or financial relationships that could be construed as a potential conflict of interest. The funding sponsors had no role in the design of the study; in the collection, analyses, or interpretation of data; in the writing of the manuscript, and in the decision to publish the results.

Appendix A. Cancellation of Adaptive Parameter Terms in the Lyapunov Proof

Substituting the control law (16) into (A1) and applying the adaptation laws (17), the z_2-related terms in $\dot{V}$ become:

$$\begin{aligned}\dot{V} = {} & e(-k_1 e + z_1) + z_1\left(-k_2 z_1 - e + \frac{A_p}{m_p} z_2\right) \\ & + z_2\left[\frac{m_p}{A_p}\left(k_2\left((\ddot{x}_r + k_1(\dot{x}_r - \dot{x}_p)\right) - \frac{A_p}{m_p} P_L\right)\right. \\ & \left. + \dot{e} + \dddot{x}_r + k_1\left(\ddot{x}_r - \frac{A_p}{m_p} P_L\right)\right) - f_1 \dot{x}_p - f_2 P_L - f_3\sqrt{P_s - sign(u)P_L}\,u \pm \hat{f}_3\sqrt{P_s - sign(u)P_L}\,u\Big] \\ & + \tilde{f}_1\Gamma_{f_1}(-\dot{\hat{f}}_1) + \tilde{f}_2\Gamma_{f_2}(-\dot{\hat{f}}_2) + \tilde{f}_3\Gamma_{f_3}(-\dot{\hat{f}}_3)\end{aligned} \tag{A1}$$

$$\begin{aligned}\dot{V}\big|_{z_2} &= z_2\Big[\hat{f}_1\dot{x}_p + \hat{f}_2 P_L + \hat{f}_3\sqrt{P_s - \mathrm{sign}(u)P_L}\,u \\ &\quad - f_1\dot{x}_p - f_2 P_L - f_3\sqrt{P_s - \mathrm{sign}(u)P_L}\,u - k_3 z_2 - \frac{A_p}{m_p} z_1\Big] \\ &= -\tilde{f}_1\dot{x}_p z_2 - \tilde{f}_2 P_L z_2 - \tilde{f}_3\sqrt{P_s - \mathrm{sign}(u)P_L}\,u\,z_2 - k_3\|z_2\|^2 - \frac{A_p}{m_p} z_1 z_2\end{aligned} \tag{A2}$$

where $\tilde{f}_i = f_i - \hat{f}_i$ denotes the parameter estimation error. Substituting these into the full expression of $\dot{V}$ in (A1) and collecting the $\tilde{f}_i$ terms together with the adaptation laws (17):

$$\begin{aligned}\dot{V} = {} & -k_1\|e\|^2 - k_2\|z_1\|^2 - k_3\|z_2\|^2 \\ & + \tilde{f}_1\Big(-\Gamma_{f_1}^{-1}\dot{\hat{f}}_1 - \dot{x}_p z_2\Big) + \tilde{f}_2\Big(-\Gamma_{f_2}^{-1}\dot{\hat{f}}_2 - P_L z_2\Big) \\ & + \tilde{f}_3\Big(-\Gamma_{f_3}^{-1}\dot{\hat{f}}_3 - \sqrt{P_s - \mathrm{sign}(u)P_L}\,u\,z_2\Big)\end{aligned} \tag{A3}$$

By direct substitution of the adaptation laws (17), each parenthesized term vanishes identically:

$$\begin{aligned} -\Gamma_{f_1}^{-1}\dot{\hat{f}}_1 - \dot{x}_p z_2 = 0 \Rightarrow \dot{\hat{f}}_1 = -\Gamma_{f_1}\dot{x}_p z_2 \\ -\Gamma_{f_2}^{-1}\dot{\hat{f}}_2 - P_L z_2 = 0 \Rightarrow \dot{\hat{f}}_2 = -\Gamma_{f_2} P_L z_2 \\ -\Gamma_{f_3}^{-1}\dot{\hat{f}}_3 - \sqrt{P_s - \text{sign}(u)P_L}\, u\, z_2 = 0 \Rightarrow \dot{\hat{f}}_3 = -\Gamma_{f_3}\sqrt{P_s - sign(u)P_L}\, u z_2 \end{aligned} \tag{A4}$$

References

1. He, Q.; Fan, X.; Ma, D. Full bicycle dynamic model for interactive bicycle simulator. *J. Comput. Inf. Sci. Eng.* **2005**, *5*, 373–380. [CrossRef]
2. Shoman, M.M.; Imine, H. Bicycle simulator improvement and validation. *IEEE Access* **2021**, *9*, 55063–55076. [CrossRef]
3. Owczarkowski, A.; Horla, D.; Kozierski, P.; Sadalla, T. Dynamic modeling and simulation of a bicycle stabilized by LQR control. In *Proceedings of the 21st International Conference on Methods and Models in Automation and Robotics (MMAR)*; Curran Associates, Inc.: New York, NY, USA, 2016; pp. 907–911.
4. Zhao, L.; Yu, Y.; Zhou, C. Dynamic modeling, simulation and experimental investigation on cycling-trainers equipped with suspensions considering human biomechanical characteristics. *J. Vibroeng.* **2020**, *22*, 1228–1239. [CrossRef]
5. Kim, G.; Lee, S.Y.; Oh, J.S.; Lee, S. Deep learning-based estimation of the unknown road profile and state variables for the vehicle suspension system. *IEEE Access* **2021**, *9*, 13878–13890. [CrossRef]
6. Imine, H.; Madani, T.; Shoman, M. Dynamic parameter identification of a bicycle using sliding mode observer and particle swarm optimization. *Highlights Veh.* **2025**, *3*, 15–29. [CrossRef]
7. Imine, H.; Fridman, L.; Madani, T. Identification of vehicle parameters and estimation of vertical forces. *Int. J. Syst. Sci.* **2015**, *46*, 2996–3009. [CrossRef]
8. Arat, M.A.; Holweg, E.; Taheri, S. Road profile estimation for active suspension applications. *SAE Int. J. Passeng. Cars Mech. Syst.* **2015**, *8*, 492–500. [CrossRef]
9. Čerškus, A.; Lenkutis, T.; Šešok, N.; Dzedzickis, A.; Viržonis, D.; Bučinskas, V. Identification of road profile parameters from vehicle suspension dynamics for control of damping. *Symmetry* **2021**, *13*, 1149. [CrossRef]
10. Yao, J.; Xiao, R.; Chen, S.; Di, D.; Gao, S.; Yu, H. Acceleration harmonic identification algorithm based on the unscented Kalman filter for shaking signals of an electro-hydraulic servo shaking table. *J. Vib. Control* **2015**, *21*, 3205–3217. [CrossRef]
11. Zhang, Z.; Sun, C.; Bridgelall, R.; Sun, M. Road profile reconstruction using connected vehicle responses and wavelet analysis. *J. Terramech.* **2018**, *80*, 21–30. [CrossRef]
12. Lenkutis, T.; Čerškus, A.; Šexsxok, N.; Dzedzickis, A.; Bučinskas, V. Road surface profile synthesis: Assessment of suitability for simulation. *Symmetry* **2021**, *13*, 68. [CrossRef]
13. Thong, Y.K.; Woolfson, M.S.; Crowe, J.A.; Hayes-Gill, B.R.; Jones, D.A. Numerical double integration of acceleration measurements in noise. *Measurement* **2004**, *36*, 73–92. [CrossRef]
14. Nan, Y.; Shao, S.; Ren, C.; Wu, K.; Cheng, Y.; Zhou, P. Simulation and experimental research on active suspension system with time-delay feedback control. *IEEE Access* **2023**, *11*, 88498–88510. [CrossRef]
15. Nguyen, T.A. Advance the efficiency of an active suspension system by the sliding mode control algorithm with five state variables. *IEEE Access* **2021**, *9*, 164368–164378. [CrossRef]
16. Wijaya, A.A.J.I.; Yakub, F.; Abdullah, S.S.; Aljazzar, S.; Kamal, M.A.S. Adaptive estimation and control of nonlinear suspension systems with natural logarithm sliding mode control. *IEEE Access* **2024**, *12*, 60896–60907. [CrossRef]
17. Ultsch, J.; Pfeiffer, A.; Ruggaber, J.; Kamp, T.; Brembeck, J.; Tobolář, J. Reinforcement learning for semi-active vertical dynamics control with real-world tests. *Appl. Sci.* **2024**, *14*, 7066. [CrossRef]
18. Kararsiz, G.; Paksoy, M.; Metin, M.; Basturk, H.I. An adaptive control approach for semi-active suspension systems under unknown road disturbance input using hardware-in-the-loop simulation. *Trans. Inst. Meas. Control* **2021**, *43*, 995–1008. [CrossRef]
19. Paksoy, M.; Metin, M. Nonlinear semi-active adaptive vibration control of a half vehicle model under unmeasured road input. *J. Vib. Control* **2019**, *25*, 2453–2472. [CrossRef]
20. Chindamo, D.; Gadola, M.; Armellin, D.; Marchesin, F. Design of a road simulator for motorcycle applications. *Appl. Sci.* **2017**, *7*, 1220. [CrossRef]
21. Chindamo, D.; Gadola, M.; Marchesin, F.P. Reproduction of real-world road profiles on a four-poster rig for indoor vehicle chassis and suspension durability testing. *Adv. Mech. Eng.* **2017**, *9*, 1687814017726004. [CrossRef]
22. Azizi, M.J.; Mirzaei, M.; Rafatnia, S.; Nodeh, T.F. Design and experimental evaluation of road excitation simulator. *J. Theor. Appl. Vib. Acoust.* **2024**, *10*, 34–49.

23. Shen, G.; Lv, G.M.; Ye, Z.M.; Cong, D.C.; Han, J.W. Feed-forward inverse control for transient waveform replication on electro-hydraulic shaking table. *J. Vib. Control* **2012**, *18*, 1474–1493. [CrossRef]
24. Metin, M.; Yılmaz, F.C.; Taşağıl, G.; Bayram, T.; Yiğit, F. Nonlinear backstepping control of a hydraulic simulator for reference road input. *Pamukkale Univ. J. Eng. Sci.* **2025**, *31*, 1–8. [CrossRef]
25. Dursun, U.; Bayram, T. Tracking control solution for road simulators: Model-based iterative learning control approach improved by time-domain modelling. *Gazi Univ. J. Sci.* **2012**, *25*, 467–477.
26. Taşağıl, G.; Başgöl, B.; Metin, M.; Bayram, T. Elastomer karakterizasyon test sistemlerinin modellenmesi ve parametrik analizleri. *Eur. J. Sci. Technol.* **2020**, *20*, 881–889. [CrossRef]
27. Taşağıl, G.; Metin, M.; Bayram, T. Hidrolik tahrikli aks mili test sisteminin adaptif bulanık PID ile kontrolü. *Mühendis ve Makina* **2023**, *64*, 17–38. [CrossRef]
28. Slotine, J.-J.E.; Li, W. *Applied Nonlinear Control*; Prentice Hall: Englewood Cliffs, NJ, USA, 1991.

Disclaimer/Publisher's Note: The statements, opinions and data contained in all publications are solely those of the individual author(s) and contributor(s) and not of MDPI and/or the editor(s). MDPI and/or the editor(s) disclaim responsibility for any injury to people or property resulting from any ideas, methods, instructions or products referred to in the content.